Validation of in-situ ionospheric density using FORMOSAT-7/COSMIC-2 IVM and ICON IVM

Jong-Min Choi
National Cheng Kung University
Charles Lin (charles@mail.ncku.edu.tw)
National Cheng Kung University https://orcid.org/0000-0001-8955-8753
P. K. Rajesh
National Cheng Kung University
Jaeheung Park
Korea Astronomy and Space Science Institute
Young-Sil Kwak
Korea Astronomy and Space Science Institute
Shih-Ping Chen
National Cheng Kung University
Jia-Ting Lin
National Cheng Kung University

Research Article

Keywords: FORMOSAT-7/COSMIC-2, ICON, IVM ion density, solar minimum, equatorial plasma bubble

Posted Date: July 5th, 2022

DOI: https://doi.org/10.21203/rs.3.rs-1758637/v1

Version of Record: A version of this preprint was published at Earth, Planets and Space on January 28th, 2023. See the published version at https://doi.org/10.1186/s40623-022-01759-3.

Abstract

We investigate the validation of in-situ ion density measurements by the ion velocity meter (IVM) onboard F7/C2 and ICON, respectively, during the solar minimum condition of December 2019 to November 2020. The diurnal variation in ion density measured by F7/C2 IVM is consistent with that of ICON IVM except for different magnitude in the December solstice. The distribution of the equatorial ion density from both satellites agrees with those observed by C/NOFS IVM satellite during the low solar activity period in 2008–2009 (Coley et al, 2010). The diurnal variation in the equatorial region did not show any effect by PRE during 2019–2020, except for observations taken at the ICON altitude during equinoxes. The plasma distributions at the low latitude depend on the season. The simultaneous observations from F7/C2 IVM and ICON IVM provide opportunities to study the spatial configuration and time evolution of ionospheric irregularity in the equatorial region and low latitude. The F7/C2 and ICON simultaneously observed the equatorial plasma bubbles (EPBs) occurring around Taiwan on 18 October 2020, and the observations are consistent with each other. The EPBs were also observed by an all-sky imager located in Taiwan for validation of the satellite observations.

Key Points

1. The diurnal variation of ion density measured by F7/C2 IVM is similar to that of ICON IVM.

2. The diurnal variation in the equatorial region did not show any effect by PRE during 2019-2020, except for observations taken at the ICON altitude during equinoxes.

3. The simultaneous observations of F7/C2 and ICON confirmed the evolution of EPBs around Taiwan, consistent with the results of the Taiwan all-sky imager.

1. Introduction

The Ion Velocity Meter (IVM) instruments onboard FORMOSAT-7/COSMIC-2 (F7/C2) constellation and Ionospheric Connection Explorer (ICON) satellite are conducting in-situ measurements of ion density in the topside F region (Immel et al., 2017; Lin et al., 2020). With the IVM mounted on each satellite, the six F7/C2 satellites can observe ionospheric irregularities events with a wide coverage. The simultaneous observations of F7/C2 IVM and ICON IVM provide unprecedented opportunities to study ionosphere dynamics and irregularities through coordinated observations from multiple satellites.

It is well known that the extreme ultraviolet (EUV) solar radiation strongly influences the generation of F region ionospheric plasma density through the production of ion-electron pairs. The plasma density increases as the sun rise and reaches a maximum around 1300–1400 LT. As the solar zenith angle increases after noon, plasma production gradually decreases. Therefore, the ionospheric plasma density is affected by solar EVU and shows a noticeable variation with a diurnal cycle. It is well known that the temporal variations of the Earth's ionosphere are ultimately linked to those of solar activity, because the main source of the ionospheric plasma is photoionization of neutrals by solar EUV and X-ray radiations.

Solar activity in the years 2007–2009 was unusually low, as evidenced by the extremely low levels of solar EUV radiation and the F10.7 index. The ionospheric response to the abnormal low solar activity has been reported and compared to that of the previous solar activity (e.g., Chen et al., 2011; Emmert et al., 2010; Heelis et al., 2009; Liu et al., 2011; Lühr and Xiong, 2010; Solomon et al., 2010). Heelis et al. (2009) reported the unusual behavior of O+/H + transition height in the Communications/Navigation Outage Forecasting System (C/NOFS) satellite and suggested that the ionosphere was significantly contracted over the period from June to August 2008. Lühr and Xiong (2010) showed that the IRI-2007 model prediction was much higher than the electron density of CHAMP (400 km in altitude) and GRACE (500 km in altitude) satellite during the solar minimum period. The F10.7 solar activity index for 2019–2020, when F7/C2 and ICON were operating normally, is similar to that of 2007–2009. In this paper, we investigate to validate the topside F region ion density of F7/C2 IVM and ICON IVM during the recent solar minimum period.

Equatorial plasma bubble (EPB) generally signifies a localized region of plasma depletion relative to the ambient plasma density. The severe ionospheric turbulence by EPB affects the path of radio waves in the ionosphere, causing problems in communication and navigation systems. After sunset, the gradient of plasma density in the bottomside F region increases steeply with altitude, affecting the growth of the Rayleigh-Taylor instability (RTI). EPB is generated from unstable ionospheres due to the growth of RTI (Kelley, 2009; Sultan 1996). The EPBs occur in the equatorial F region after sunset and are elongated along the magnetic field lines (e.g., Kil et al., 2004; Martinis and Mendillo, 2007). The C/NOFS satellite operated in a low inclination (13°) and elliptical (400–800 km) orbit during 2008–2015. In-situ satellite measurements of C/NOFS IVM conducted the characteristics and generation of EPB during the long solar minimum (e.g. Huang et al., 2013; 2014; Huang, 2017; Kil et al., 2011a; 2015). The EPB occurrence rates are maximum for 20–22 LT (e.g. Su et al., 2006). However, strong postmidnight EPBs are also observed during the June solstice of the solar minimum (e.g., Hei et al., 2014; Yizengaw et al., 2009; 2013).

The F7/C2 was launched on 25 June 2019 into a low inclination (24°) at ~ 550 km altitude (Lin et al., 2020). The ICON was launched on 11 October 2019. The satellite has a circular low inclination orbit (27°) at an altitude of ~ 600 km (Immel et al., 2017). F7/C2 IVM and ICON IVM measured the ion density, velocities, temperature, and composition (Heelis et al., 2017). We used total ion density from the December 2019 to November 2020. To cross-validate the data of the two satellites, we compare diurnal, seasonal and latitudinal variations of the ionospheric density and EPB at low latitude. The data selection for this paper is described in section 2. The observation results are given in sections 3.1 and 3.2. Finally, we draw our main conclusions in section 4.

2. Data Selection

To validate the in-situ ion densities obtained from the IVM onboard equatorial satellite#1 of F7/C2 (simplified as F7/C2E1) and ICON, respectively, we investigate the diurnal variation of ion density from December 2019 to November 2020 and the EPBs around Taiwan on 18 October 2020. In 2019–2020 the solar radio flux is observed to be extremely low. Figure 1 shows the daily averaged F10.7 and Kp index.

The solar flux was kept at small values (< 100 sfu) in 2018–2020, and its magnitude is similar to the low solar flux in 2008–2010. In the fall of 2020, the solar flux increased to 100, and then it seems to rise slightly. In section 3.1, we selected magnetically quiet time (Kp ≤ 3) ion density detected during solar minimum period from the December 2019 to November 2020 to identify the diurnal variation of ion density observed by F7/C2E1 and ICON. Figure 2 shows the data availability distributions of F7/C2E1 data (red) and ICON data (blue) as a function of local time (1 hour bin) for the June solstice (May, June, July, and August: top panel), Equinox (March, April, September, and October: middle panel), and the December solstice (November, December, January, and February: bottom panel). The F7/C2E1 IVM and ICON IVM have a uniform data distribution with respect to time.

3. Results And Discussions

3.1. Diurnal variation of ion density

Figure 3 depicts the behavior of the ion density with local time. The diurnal variations of ion density are shown in three seasons: June solstice (May, June, July, and August: middle panel), Equinox (March, April, September, and October: bottom panel), December solstice (November, December, January, and February: top panel) during the solar minimum of the December 2019 to November 2020. The local time is binned by 1 hour, and the plot shows median ion density measured by F7/C2E1 (blue lines) and ICON (black lines). The ion density in the F region decreases at night and increases during the day, which is due to photoionization by solar EUV radiation and diurnal variations of the electromagnetic drifts (i.e. $E \times B$ drifts) that transport plasma to a higher altitude during the day and to lower altitude at night (e.g., Schunk and Nagy, 1978; 2000, Anderson et al., 2004). The diurnal variation pattern of ion density is characterized by remarkable one peak values, occurring in the noon hours around 10:00–14:00 LT. The local time dependence of ion density measured by F7/C2E1 IVM is similar to that measured by ICON. The magnitude of ion density during noon hours has a maximum value in the December solstice and a minimum value in the June solstice. Also, the ion density of Equinoxes is greater than that of June solstice. The ionosphere plasma density is determined by the plasma production, loss, and transport processes. Plasma production and loss are affected by EUV and recombination, respectively. Since the recombination is affected by thermospheric neutral density and the hemispheric wind effect, various factors drive the seasonal variation in plasma density. The difference in ion density resulting from the hemispheric wind effect will be discussed in Fig. 4.

In Fig. 3, nighttime ion density observed by ICON IVM is slightly greater than F7/C2E1 IVM, but vice versa during daytime. During the data period from 2019 to 2020, the ICON altitude (550–600 km) is about 50 km higher than the F7/C2E1 altitude (500–550 km). An altitude difference of 50 km between F7/C2E1 altitude and ICON altitude may cause a difference in density between F7/C2E1 and ICON. The solar EUV radiation changing with solar zenith angle plays a significant role in ion production in the ionosphere during daytime. After the solar EUV radiation disappears during nighttime, recombination has an important role in ion density. A slight difference in height causes a difference in these two processes, resulting in a difference in ion density. Interestingly, the difference in density between the two satellites is

maximized during 10–17 LT in December. The ICON densities do not vary significantly with the season, but F7/C2E1 densities increase significantly during the daytime only in the December solstice. If the velocity data of F7/C2E1 is fully calibrated in the future, it will be possible to identify the cause of this difference.

The ion density variation with local time is different depending on the season, and it also have a dependence on solar activity. In the diurnal variation of the ion density measured by F7/C2E1 and ICON during the low solar activity from December 2019 to November 2020, no increase in density due to pre-reversal enhancement (PRE) was observed. Xiong et al., (2016) reported the diurnal variation of electron density observed from Swarm A and C during moderate solar activity from April 2014 to April 2016. In Fig. 4(b) of Xiong et al. (2016), the electron density in the equinox measured by the Swarm increases rapidly near sunset (1700–1900 LT) because of the PRE effect. However, this characteristic is absent in the ion density measured by F7/C2E1 and ICON.

The seasonal and solar activity variations of evening PRE have been reported by several literatures (Fejer et al., 1981; 1991; 2008; Kil et al. 2007, 2009). The PRE magnitude of the vertical plasma drift tends to increase with solar flux (Fejer et al., 1991; 1999; Kil et al., 2011b). The magnitude has also a dependence on seasonal variation, reaching its maximum during the equinox and its minimum during the June solstice (e.g. Fesen et al., 2000). The PRE can uplift the height of the equatorial F region, making a favorable condition for EPB development. The reduced ion-neutral collision frequency at higher altitudes has a positive effect on the growth of Rayleigh-Taylor instability associated with EPB generation.

The solar activity dependence of the EPB occurrence probability was investigated based on the in-situ satellite measurements of DMSP during 1989–2004 (Huang et al., 2002; Gentile et al., 2006)d NOFS during – 2008–2014 (Huang et al., 2015) and CHAMP and GRACE during 2001–2009 (Xiong et al., 2010). More EPBs occur at a higher solar activity. The F7/C2 and ICON may observe relatively fewer EPBs during the solar minimum condition from December 2019 to November 2020, but can still provide opportunities to study the seeding effect from the lower altitude. We will introduce an example of the EPB observed through the simultaneous observations of ICON and F7/C2 in section 3.2.

Figure 4 presents the local time variation of the averaged ion density for three different seasons at the equatorial (± 5°) and low latitude (± 10° to ± 20°) regions to characterize the structure of EIA. Regardless of latitude and season variation, the patterns of ion density measured by both satellites are similar, but the densities at F7/C2E1 altitudes appear to be greater than or nearly identical to those of ICON. Coley et al. (2010) reported the ion density observed by C/NOFS IVM during the summer of 2008. The ion density range of C/NOFS at an altitude of 500–550 km is consistent with that of F7/C2E1 and ICON shown in this study. The difference in density between the two satellites was clearly observed during the daytime of the equatorial region, where the densities of Equinoxes and December solstice are greater than those of June solstice. The density of the ICON altitude increases rapidly before 1800 LT in the equatorial region of Equinox, which appears to be due to the PRE. However, this effect is not seen at the F7/C2E1 altitude, which may indicate a difference in altitude of the PRE effect.

We separated the data into the southern and northern hemispheres to compare the ion density distributions obtained from both satellites in low latitude regions. The low latitude F7/C2E1 densities between 1200-1400LT are roughly a similar distribution, but there is a clear difference in the southern hemisphere of the December solstice. Since the summer-to-winter winds during solstice affects the plasma motion and ionospheric morphology (Rishbeth et al., 2000; Lin et al., 2007), the F region neutral wind has a significant effect in the hemispheric asymmetry of the topside ionosphere. West et al. (1997) examined variations in ion composition associated with solar activity using DMSP F10 and concluded that F region neutral winds cause modulation of the F peak height, which is responsible for the hemispheric asymmetry of the topside ionosphere. Su et al. (1998) showed that the electron density obtained by the Hinotori satellite revealed an effect of ion drag on the meridional wind. Further, Kil et al. (2006) suggested that equatorial winds stand against downward plasma diffusion, resulting in hemispheric asymmetry of the topside ionosphere at an altitude of 840 km. The summer-to-winter winds are equatorward (poleward) at the summer (winter) hemisphere preventing (accelerating) the downward diffusion of the plasma at topside. The process results in stronger topside density at the summer hemisphere than the winter hemisphere. Kwak et al. (2019) presented the hemispheric asymmetry of EIA with solar cycle is associated with the fountain process and interhemispheric wind. In Fig. 4c, the density of the southern hemisphere (summer) is larger than those of the northern hemisphere (winter), which can be interpreted as the hemispheric wind effect during the December solstice. The summer and winter hemisphere asymmetry is more prominent during the December solstice than the June solstice, which is consistent to the annual asymmetry of the ionosphere (Millward et al., 1996; Rishbeth. and Müller-Wodarg, 2006). The more prominent annual asymmetry effect in the December solstice may cause differences in the density values of F7/C2E1 and ICON during the daytime (10–17 LT) in Fig. 3c. However, the hemispheric wind effect in the June solstice had less influence on the distribution of ion density (Fig. 3a, Fig. 4a).

The morphology of topside plasma density has been reported in several literatures, and it differs from the F peak height (Su et al., 1998; Kil et al., 2006; Liu et al., 2007). Figure 5 shows the distribution of averaged ion density on the topside F region as a function of magnetic latitude observed by (left) F7/C2E1 and (right) ICON for three seasons. The ion density measurements from F7/C2E1 and ICON are sorted into local time (1 h) by magnetic latitude (5◦) bins. The ion density at low latitude is higher during the Equinox and December solstice than during the June solstice. The rapid increase of the density of the ICON altitude before 1800 LT in the equatorial region of Equinox, which appears to be due to the PRE, is also confirmed. The topside ion density of ICON altitude and F7/C2E1 altitude did not show off-equatorial maxima in both hemispheres by the equatorial plasma fountain effect. The F7/C2E1 density has a similar distribution to the ICON density, but its amplitude appears to be stronger. Lee et al. (2011) investigated the F region electron density obtained from FORMOSAT-3/COSMIC in 2007 and showed that although the EIA peaks in both hemispheres were observed due to the fountain effect at the F peak height, the EIA structures of the southern and northern hemispheres at the 500 km altitude could not be clearly distinguished under solar minimum condition.

3.2. Simultaneous observations of equatorial plasma bubble (EPB)

In this section, we examine the EPB through the simultaneous observations of ICON and F7/C2 on 18 October 2020. The ICON altitude and F7/C2 altitude on those days were near 600 km and 550 km, respectively. Figure 6 presents a series of four consecutive ion density measurements derived from ICON and F7/C2 on 18 October 2020, showing the spatial characteristics and time evolution of EPBs. When ICON passed around Taiwan at sunset, the three F7/C2 satellites (named hereafter F7/C2E1-F7/C2E3) also performed simultaneous observations around EPBs. Figure 6a shows the longitude-latitude trajectory of ICON (blue), F7/C2E1 (magenta), F7/C2E2 (cyan), F7/C2E3 (yellow) around 2100 LT, and F7/C2E4 (green) around 2200 LT, respectively. The black dashed line represents the magnetic equator. In Figs. 6b-6e, the black curve is ion density measured by the IVM onboard each satellite. In order to calculate the smooth background density (red curve), we first applied the function of a Savitzky-Golay low-pass filter (order = 3, window size = 51 data points). Then, the smoothing process was repeated for the low-pass filter values using 50 data points running average to remove small-scale fluctuations (e.g., Kil et al. 2011, Choi et al., 2017, Smith and Heelis, 2018, Smith et al., 2018).

ICON detected an ion density depletion at sunset (Fig. 6b). The trajectory of ICON is located at low latitude in the evening sector, and its altitude is 550 km. A series of bubbles are detected in the longitude region 105°-130°E. The EPBs morphology observed by (b) ICON is almost identical to that of (c) F7/C2E1. The (d) F7/C2E2 observed the EPBs at the longitude at which ICON observed the bubble. The EPBs are developed at the magnetic equator and expand to lower latitudes along the magnetic field lines. From the comparison between (b) ICON and (d) F7/C2E2, it can be confirmed that the bubble observed near the magnetic equator extends around Taiwan. Around 2100 LT, F7/C2E3 observed the EPBs in the opposite hemisphere, which means that the bubble expands along the magnetic field lines into the opposite hemisphere.

Plasma bubbles have been observed using an all-sky imager by National Cheng Kung University at Tainan Astronomical and Educational Area (23.1°N, 120.4°E) in Taiwan (Rajesh et al., 2017). On 18 October 2020, the all-sky imager observations were restricted by cloudy weather, but plasma bubbles were detected in some images. Figure 7 presents the coincident observations of plasma bubble over Taiwan (a) 2230 LT and (b) 2236 LT on the night of October 18, 2020. The airglow images in Fig. 7 are unwrapped into geographic coordinates, assuming an emission height of 250 km (Rajesh et al., 2017). The F7/C2E3 orbit tracks are mapped to low latitudes at an altitude of 250 km along magnetic field lines. The F7/C2E3 orbit and ion density are shown with green and red curves in Fig. 7, respectively. A different series of plasma bubbles were detected in comparison to the previous orbit in the longitude 110°-130°E. OI 630.0-nm airglow images show plasma bubbles as band-like airglow depletions (blue dashed box) that are elongated in the north-south direction. The dark bands of airglow images correspond to plasma bubbles observed in the F7/C2E3 orbit.

4. Conclusions

In this paper, in-situ ion densities measurements from IVM onboard F7/C2E1 and ICON, respectively, were validated by comparing observations during magnetic quiet days of the solar minimum period from December 2019 to November 2020. The diurnal variation of ion density of the F7/C2E1 is similar to that of ICON for the three seasons. The daytime electron density has maxima around the December solstice and minima around the June solstice. F7/C2 density at the equatorial region did not show any effect by PRE during the solar minimum period (December 2019 to November 2020), but ICON density increases rapidly around sunset in Equinoxes. The hemispheric asymmetry of the topside ionosphere at low latitude regions is comparable for F7/C2E1 and ICON during the June solstice and Equinoxes, while the F7/C2E1 density is larger during the December solstice. The simultaneous observations of the F7/C2 and ICON confirm the evolution of EPBs around Taiwan. The EPBs expanded from the geomagnetic equator to the low latitude and from the northern hemisphere to the southern hemisphere. The EPBs observed from F7/C2E3 corresponds to the dark band of the all-sky imager. The F7/C2 IVM and ICON IVM provide topside ion density with good performance, and this is confirmed in this study through the statistical analysis and an event study. The ion density data from the F7/C2 IVM and ICON IVM allow -providing opportunities for understanding the characteristics of ionospheric irregularity and its evolution during the solar minimum.

Declarations

Availability of data and materials

The F7/C2 IVM data is downloaded from the website of the Taiwan Analysis Center for COSMIC (TACC, https://tacc.cwb.gov.tw/data-service/fs7_provisional/level2/ivmL2m/) or the University Corporation for Atmospheric Research (UCAR, https://data.cosmic.ucar.edu/gnss-ro/cosmic2/postProc/level2/). The ICON IVM data are available from ftp://icon-science.ssl.berkeley.edu/pub/LEVEL.2/IVM-A/. F10.7 and Kp index were obtained from the OMNIWEB database (https://omniweb.gsfc.nasa.gov/ow.html). Access of all sky images is at http://allsky-airglow.earth.ncku.edu.tw/PicWeb/MainHTML/2020/10/18.

Competing interests

Not applicable.

Funding

This work is partly supported by the Ministry of Science and Technology under MOST 110-2111-M-006-004 and MOST 110-2119-M-006-001, National Space Organization under NSPO-S-110296, and the Headquarter of University Advancement at National Cheng Kung University, which is sponsored by the Taiwan Ministry of Education under grant number D111-G2205. J. Park and Y.-S. Kwak were supported by basic research funding from the Korea Astronomy and Space Science Institute (KASI)

(KASI2022185009).J. Park and Y.-S. Kwak were supported by basic research funding from the Korea Astronomy and Space Science Institute (KASI) (KASI2022185009).

Authors' contributions

JC conducted data analysis and wrote the first draft of the manuscript. CCL designed this study and helped the interpretation of the results. PKR supported the Taiwan all-sky imager data analysis. JP supported the satellites data analysis and discussion of data characteristics. YK contributed to the interpretation of the results. SC managed the F7/C2 satellite data and helped the data analysis. JL operated the Taiwan all-sky imager. All authors read and approved the final manuscript.

Acknowledgements

JC thanks the staff at the National Cheng Kung University for proving the F7/C2 data and Taiwan all-sky imager data. JC also thanks the ICON Team.

Authors details

1Department of Earth Sciences, National Cheng Kung University, Tainan, Taiwan. 2Korea Astronomy and Space Science Institute, Daejeon, South Korea. 3University of Science and Technology, Daejeon, South Korea

References

1. Anderson D, Anghel A, Chau JL, Veliz O (2004) Daytime vertical E × B drift velocities inferred from ground-based magnetometer observations at low latitudes. Space Weather 2:S11001. doi:10.1029/2004SW000095
2. Chen Y, Liu L, Wan W (2011) Does the F10.7 index correctly describe solar EUV flux during the deep solar minimum of 2007–2009? J Geophys Res 116:A04304. doi:10.1029/2010JA016301
3. Choi J-M, Kil H, Kwak Y-S, Park J, Lee WK, Kim YH (2017) Periodicity in the occurrence ofequatorial plasma bubbles derived fromthe C/NOFS observations in 2008–2012. J Geophys Res Space Physics 122:1137–1145. doi:10.1002/2016JA023528
4. Coley WR, Heelis RA, Hairston MR, Earle GD, Perdue MD, Power RA, Harmon LL, Holt BJ, Lippincott CR (2010) Ion temperature and density relationships measured by CINDI from the C/NOFS spacecraft during solar minimum. J Geophys Res 115:A02313. doi:10.1029/2009JA014665
5. Emmert JT, Lean JL, Picone JM (2010) Record low thermospheric density during the 2008 solar minimum. Geophys Res Lett 37:L12102. doi:10.1029/2010GL043671
6. Fejer BG, Farley DT, Gonzales CA, Woodman RF, Calderon C (1981) F region east-west drifts at Jicamarca. J Phys Res 86(A1):215–218. doi:10.1029/JA086iA01p00215
7. Fejer BG, de Paula ER, Gonzales SA, Woodman RF (1991) Average vertical and zonal F region plasma drifts over Jicamarca. J Geophys Res 96(A8):13901–13906. doi:10.1029/91JA01171

8. Fejer BG, Scherliess L, de Paula ER (1999) Effects of the vertical plasma drift velocity on the generation and evolution of equatorial spread F. J Geophys Res 104(A9). doi:10.1029/1999JA900271
9. Fejer BG, Jensen JW, Su SY (2008) Quiet time equatorial F region vertical plasma drift model derived from ROCSAT-1 observations. J Phys Res 113:A05304. doi:10.1029/2007JA012801
10. Fesen CG, Crowley G, Roble RG, Richmond AD, Fejer BG (2000) Simulation of the pre-reversal enhancement in the low latitude vertical ion drifts. Geophys Res Lett 27(13):1851–1854. https://doi.org/10.1029/2000GL000061
11. Gentile LC, Burke WJ, Rich FJ (2006) A climatology of equatorial plasma bubbles from DMSP 1989–2004, Radio Sci. 41:RS5S21. 10.1029/2005RS003340
12. Heelis RA, Coley WR, Burrell AG, Hairston MR, Earle GD, Perdue MD, Power RA, Harmon LL, Holt BJ, Lippincott CR (2009) Behavior of the O+/H + transition height during the extreme solar minimum of 2008. Geophys Res Lett 36.
L00C03
.. doi:10.1029/2009GL038652
13. Heelis RA, Stoneback RA, Perdue MD, Depew MD, Morgan WA, Mankey MW et al (2017) Ion velocity measurements for the ionospheric connections explorer. Space Sci Rev 212:615–629. https://doi.org/10.1007/s11214-017-0383-3
14. Hei MA et al (2014) Radio-tomographic images of postmidnight equatorial plasma depletions. Geophys Res Lett 41:13–19. doi:10.1002/2013GL056112
15. Huang CY, Burke WJ, Machuzak JS, Gentile LC, Sultan PJ (2002) Equatorial plasma bubbles observed by DMSP satellites during a full solar cycle: Toward a global climatology. J Geophys Res 107(A12):1434. doi:10.1029/2002JA009452
16. Huang C-S, de La Beaujardière O, Roddy PA, Hunton DE, Ballenthin JO, Hairston MR, Pfaff RF (2013) Large-scale quasiperiodic plasma bubbles: C/NOFS observations and causal mechanism. J Geophys Res Space Physics 118:3602–3612. doi:10.1002/jgra.50338
17. Huang C-S, de La Beaujardiere O, Roddy PA, Hunton DE, Liu JY, Chen SP (2014) Occurrence probability and amplitude of equatorial ionospheric irregularities associated with plasma bubbles during low and moderate solar activities (2008–2012). J Geophys Res Space Physics 119:1186–1199. doi:10.1002/2013JA019212
18. Huang C-S, Hairston MR, NOFSsatellite (2015)J. Geophys. Res. Space Physics, 120,2263–2275. doi:10.1002/2014JA020735
19. Huang C-S (2017) The characteristics and generation mechanism of small-amplitude and large-amplitude ESF irregularities observed by the C/NOFS satellite. J Geophys Res Space Physics 122(8973):8959. doi:10.1002/2017JA024041
20. Immel TJ, England SL, Mende SB, Heelis RA, Englert CR, Edelstein J, Sirk MM (2017) The ionospheric connection explorer mission: Mission goals and design. Space Sci Rev 214(1):13. https://doi.org/10.1007/s11214-017-0449-2

21. Kelley MC (2009) The Earth's ionosphere: Plasma physics and electrodynamics. Elsevier, Oxford, UK
22. Kil H, Su S-Y, Paxton LJ, Wolven BC, Zhang Y, Morrison D, Yeh HC (2004) Coincident equatorial bubble detection by TIMED/GUVI and ROCSAT-1. Geophys Res Lett 31:L03809. doi:10.1029/2003GL018696
23. Kil H, DeMajistre R, Paxton LJ, Zhang Y (2006) Nighttime Fregion morphology in the low and middle latitudes seen from DMSP F15 and TIMED/GUVI. J Atmos Sol Terr Phys 68:1672–1681. doi:10.1016/j.jastp.2006.05.024
24. Kil H, Oh S-J, Kelley MC, Paxton LJ, England SL, Talaat E, Min K-W, Su S-Y (2007) Longitudinal structure of the vertical E × B drift and ion density from ROCSAT-1. Geophys Res Lett 34:L14110. doi:10.1029/2007GL030018
25. Kil H, Paxton LJ, Oh S-J (2009) Global bubble distribution seen from ROCSAT-1 and its association with the evening prereversal enhancement. J Geophys Res 114:A06307. doi:10.1029/2008JA013672
26. Kil H, Choi H-S, Heelis RA, Paxton LJ, Coley WR, Miller ES (2011a) Onset conditions of bubbles and blobs: A case study on 2 March 2009. Geophys Res Lett 38:L06101. doi:10.1029/2011GL046885
27. Kil H, Oh S-J (2011b) Dependence of the evening prereversal enhancement of the vertical plasma drift on geophysical parameters. J Geophys Res 116:A05311. doi:10.1029/2010JA016352
28. Kil H, Kwak Y-S, Lee WK, Miller ES, Oh S-J, Choi H-S (2015) The causal relationship between plasma bubbles and blobs in the low-latitude F region during a solar minimum. J Geophys Res Space Physics 120:3961–3969. doi: 10.1002/2014JA020847
29. Kwak YS, Kil H, Lee WK, Yang T-Y (2019) Variation of the Hemispheric Asymmetry of the Equatorial Ionization Anomaly with Solar Cycle. J Astronomy Space Sci 36(3):159–168. doi:10.5140/JASS.2019.36.3.159
30. Lee WK, Kil H, Kwak Y-S, Wu Q, Cho S, Park JU (2011) The winter anomaly in the middle-latitude F region during the solar minimum period observed by the Constellation Observing System for Meteorology, Ionosphere, and Climate. J Geophys Res 116:A02302. doi:10.1029/2010JA015815
31. Lin CH, Liu JY, Fang TW, Chang PY, Tsai HF, Chen CH, Hsiao CC (2007) Motions of the equatorial ionization anomaly crests imaged by FORMOSAT-3/COSMIC. Geophys Res Lett 34:L19101. doi:10.1029/2007GL030741
32. Lin C-Y, Lin CC-H, Liu J-Y et al (2020) The early results and validation of FORMOSAT-7/COSMIC-2 space weather products: Global ionospheric specification and Ne-aided Abel electron density profile. J Geophys Res : Space Physics 125:1–12 e2020JA028028. https://doi.org/10.1029/2020JA028028
33. Liu L, Wan W, Yue X, Zhao B, Ning B, Zhang M-L (2007) The dependence of plasma density in the topside ionosphere on solar activity level. Ann Geophys 25(6):1337–1343. doi:10.5194/angeo-25-1337-2007
34. Liu L, Le H, Chen Y, He M, Wan W, Yue X (2011) Features of the middle- and low-latitude ionosphere during solar minimum as revealed from COSMIC radio occultation measurements. J Phys Res 116:A09307. doi:10.1029/2011JA016691

35. Lühr H, Xiong C (2010) IRI-2007 model overestimates electron density during the 23/24 solar minimum. Geophys Res Lett 37:L23101. doi:10.1029/2010GL045430
36. Martinis C, Mendillo M (2007) Equatorial spread F-related airglow depletions at Arecibo and conjugate observations. J Geophys Res 112:A10310. doi:10.1029/2007JA012403
37. Millward GH, Rishbeth H, Fuller-Rowell TJ, Aylward AD, Quegan S, Moffett RJ (1996) Ionospheric f 2 layer seasonal and semiannual variations. J Phys Res 101(A3):5149–5156. https://doi.org/10.1029/95JA03343
38. Rajesh PK, Lin CH, Chen CH, Chen WH, Lin JT, Chou MY, Chang MT, You CF (2017) Global equatorial plasma bubble growth ratesusing ionosphere data assimilation,J. Geophys. Res Space Physics 122:3777–3787. doi:10.1002/2017JA023968
39. Rishbeth H, Müller-Wodarg ICF, Zou L, Fuller-Rowell TJ, Millward GH, Moffett RJ et al (2000) Annual and semiannual variations in the ionospheric F2-layer: II. Physical discussion. Ann Geophys 18(8):945–956. https://doi.org/10.1007/s00585-000-0945-6
40. Rishbeth H, Müller-Wodarg ICF (2006) Why is there more ionosphere in January than in July? The annual asymmetry in the F2-layer. Ann Geophys 24:3293–3311. https://doi.org/10.5194/angeo-24-3293-2006
41. Schunk RW, Nagy AF (1978) Electron temperatures in the F region of the ionosphere: Theory and observations. Rev Geophys 15:355–399
42. Schunk RW, Nagy AF (2000) Ionospheres, Physics, Plasma Physics and Chemistry. Cambridge, New York, pp 254–264
43. Smith JM, Heelis RA (2018) The plasma environment associated with equatorial ionospheric irregularities. J Geophys Research: Space Phys 123:1583–1592. doi:10.1002/2017JA024933
44. Smith JM, Heelis RA (2018) Plasma dynamics associated with equatorial ionospheric irregularities. Geophys Res Lett 45. doi:10.1029/2018GL078560
45. Solomon SC, Woods TN, Didkovsky LV, Emmert JT, Qian L (2010) Anomalously low solar extreme-ultraviolet irradiance and thermospheric density during solar minimum. Geophys Res Lett 37:L16103. doi:10.1029/2010GL044468
46. Su S-Y, Liu CH, Ho HH, Chao CK (2006) Distribution characteristics of topside ionospheric density irregularities: Equatorial versus midlatitude regions. J Geophys Res 111:A06305. doi:10.1029/2005JA011330
47. Su YZ, Bailey GJ, Oyama K-I (1998) Annual and seasonal variations in the low-latitude topside ionosphere. Ann Geophys 16:974–985. doi:10.1007/s00585-998-0974-0
48. Sultan PJ (1996) Linear theory and modeling of the Rayleigh-Taylor instability leading to the occurrence of equatorial spread F. J Phys Res 101(A12):875–926. https://doi.org/10.1029/96JA00682
49. West KH, Heelis RA, Rich FJ (1997) Solar activity variations in the composition of the low-latitude topside ionosphere. J Geophys Res 102(A1):295–305. doi:10.1029/96JA03031

50. Xiong C, Park J, Lühr H, Stolle C, Ma SY (2010) Comparing plasma bubble occurrence rates at CHAMP and GRACE altitudes during high and low solar activity. Ann Geophys 28:1647–1658. doi:10.5194/angeo-28-1647-2010
51. Xiong C, Zhou Y-L, Lühr H, Ma S-Y (2016) Diurnal evolution of the F region electron density local time gradient at low and middle latitudes resolved by the Swarm constellation. J Geophys Res Space Physics 121:9075–9089. doi:10.1002/2016JA023034
52. Yizengaw E, Moldwin MB, Sahai Y, de Jesus R (2009) Strong postmidnight equatorial ionospheric anomaly observations during magnetically quiet periods. J Geophys Res 114:A12308. doi:10.1029/2009JA014603
53. Yizengaw E, Retterer J, Pacheco EE, Roddy P, Groves K, Caton R, Baki P (2013) Postmidnight bubbles and scintillations in the quiet-time June solstice. Geophys Res Lett 40:5592–5597. doi:10.1002/2013GL058307

Figures

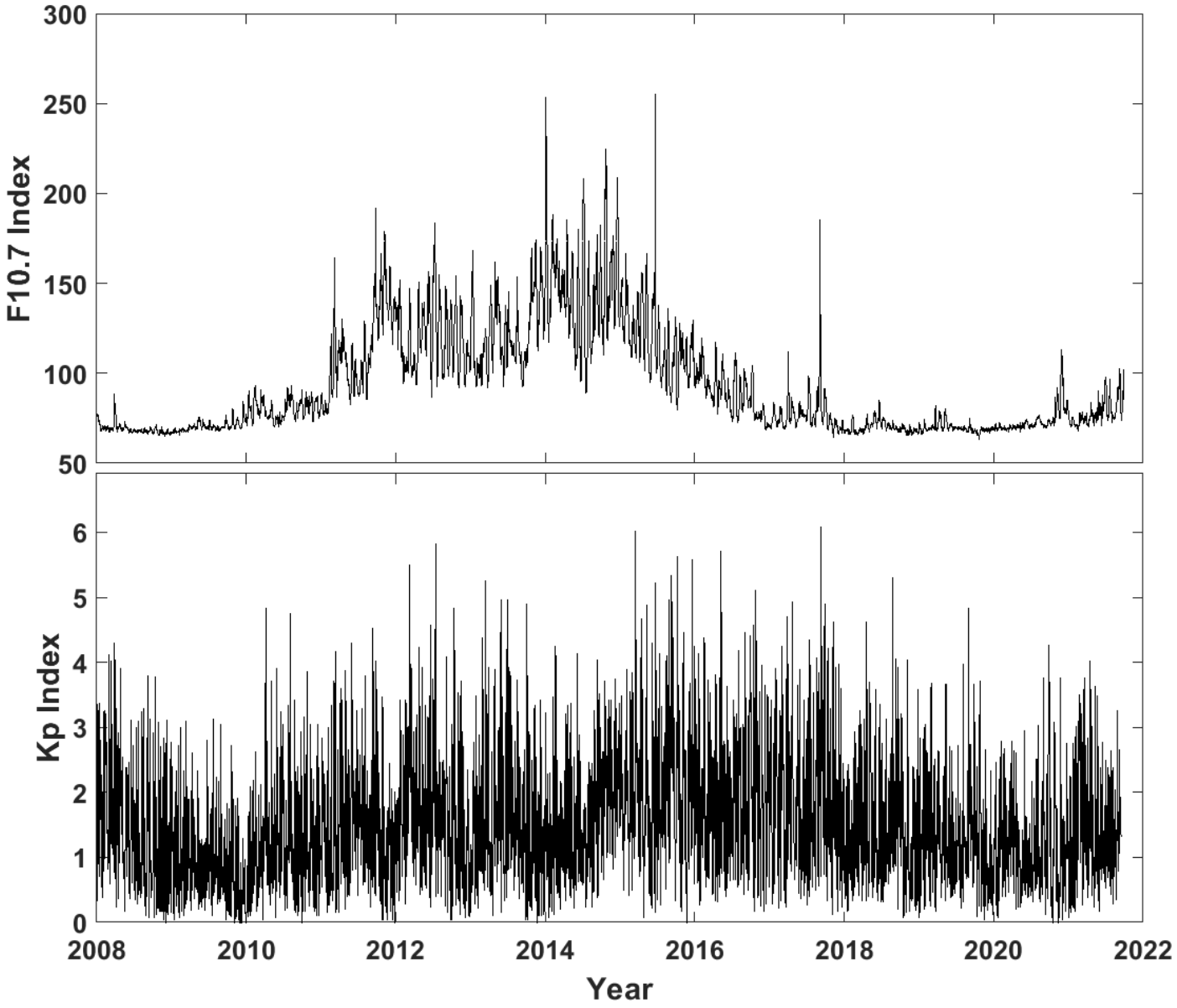

Figure 1

The solar radio flux F10.7 and Kp index variations during 2008-2021.

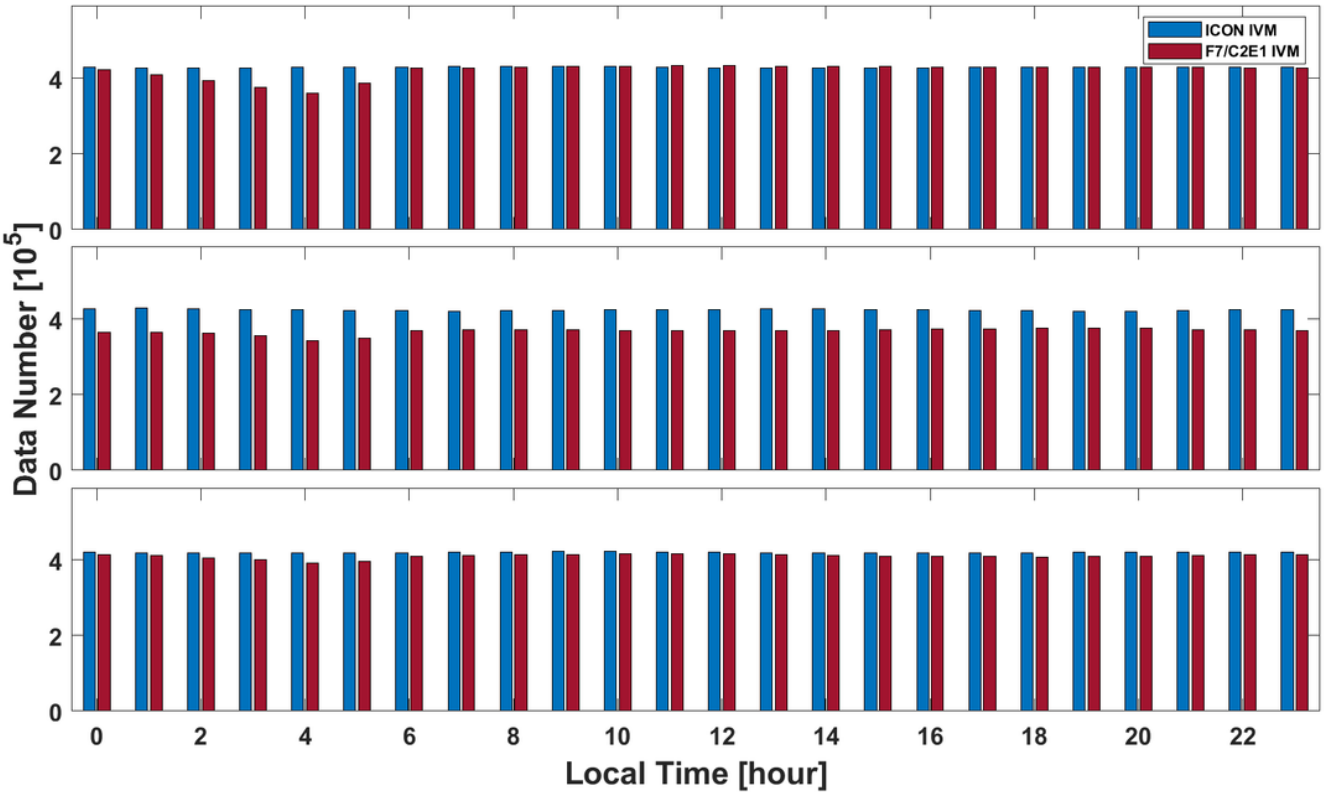

Figure 2

Seasonal and local time distribution of data availability of F7/C2E1 and ICON during the solar minimum from December 2019 to November 2020.

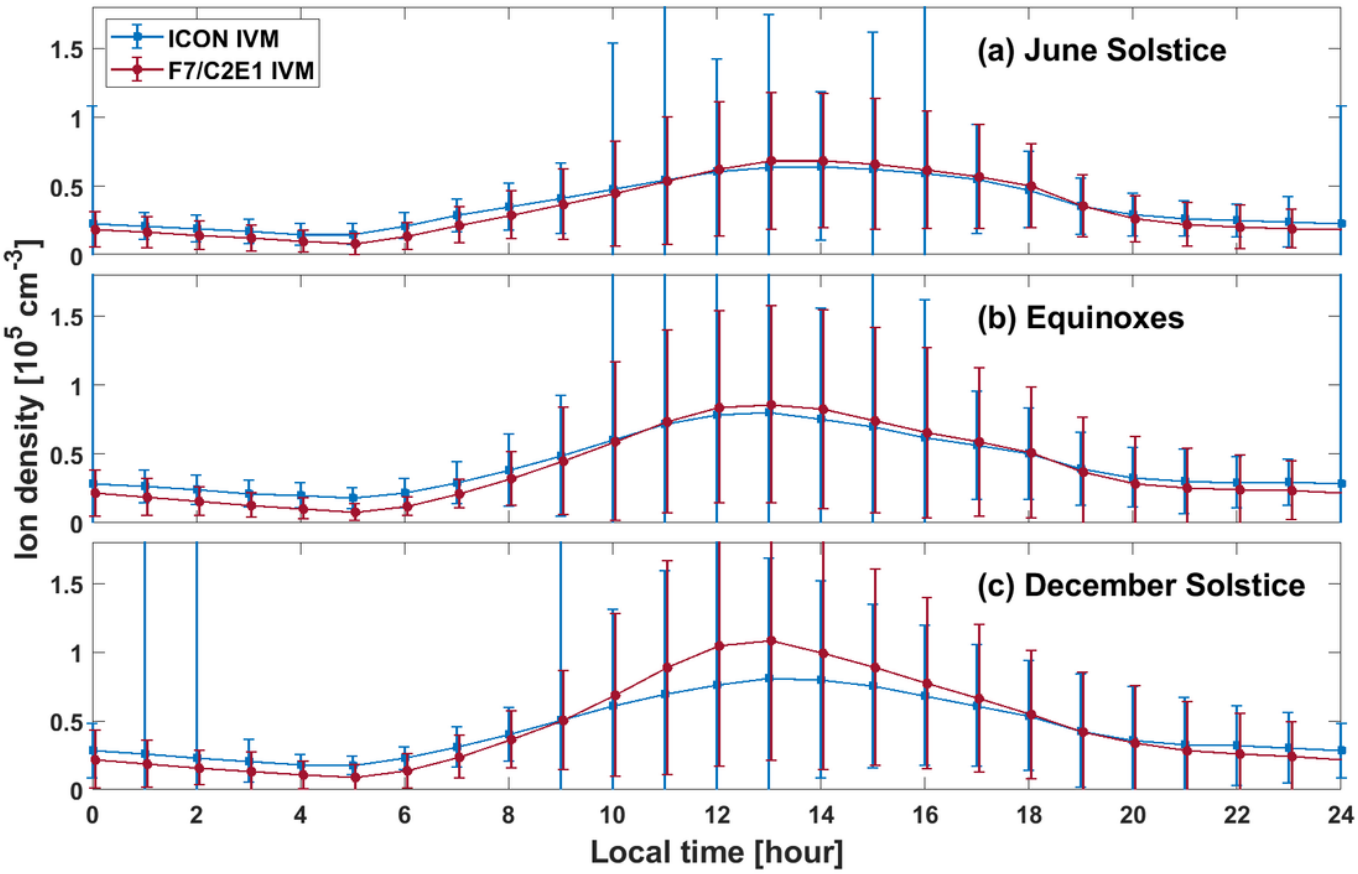

Figure 3

Diurnal variations of the ion density observed by F7/C2E1 and ICON satellite during the solar minimum period (December 2019 to November 2020) for three seasons. The error bars indicate the standard deviation.

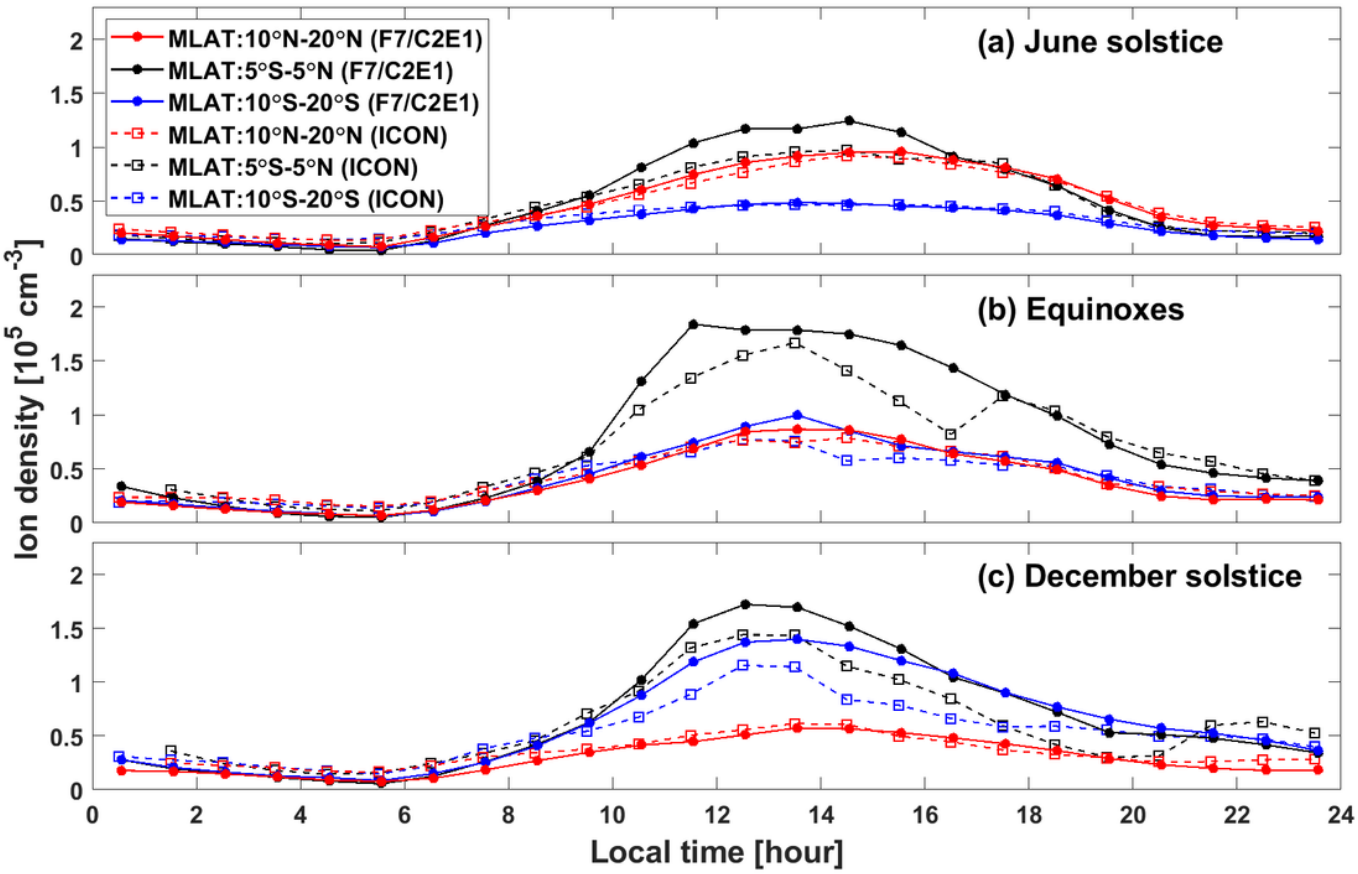

Figure 4

Comparison of the averages of the observed ion densities by F7/C2E1 (blue) and ICON (black) at various magnetic latitude ranges for June solstice, Equinoxes, and December solstice.

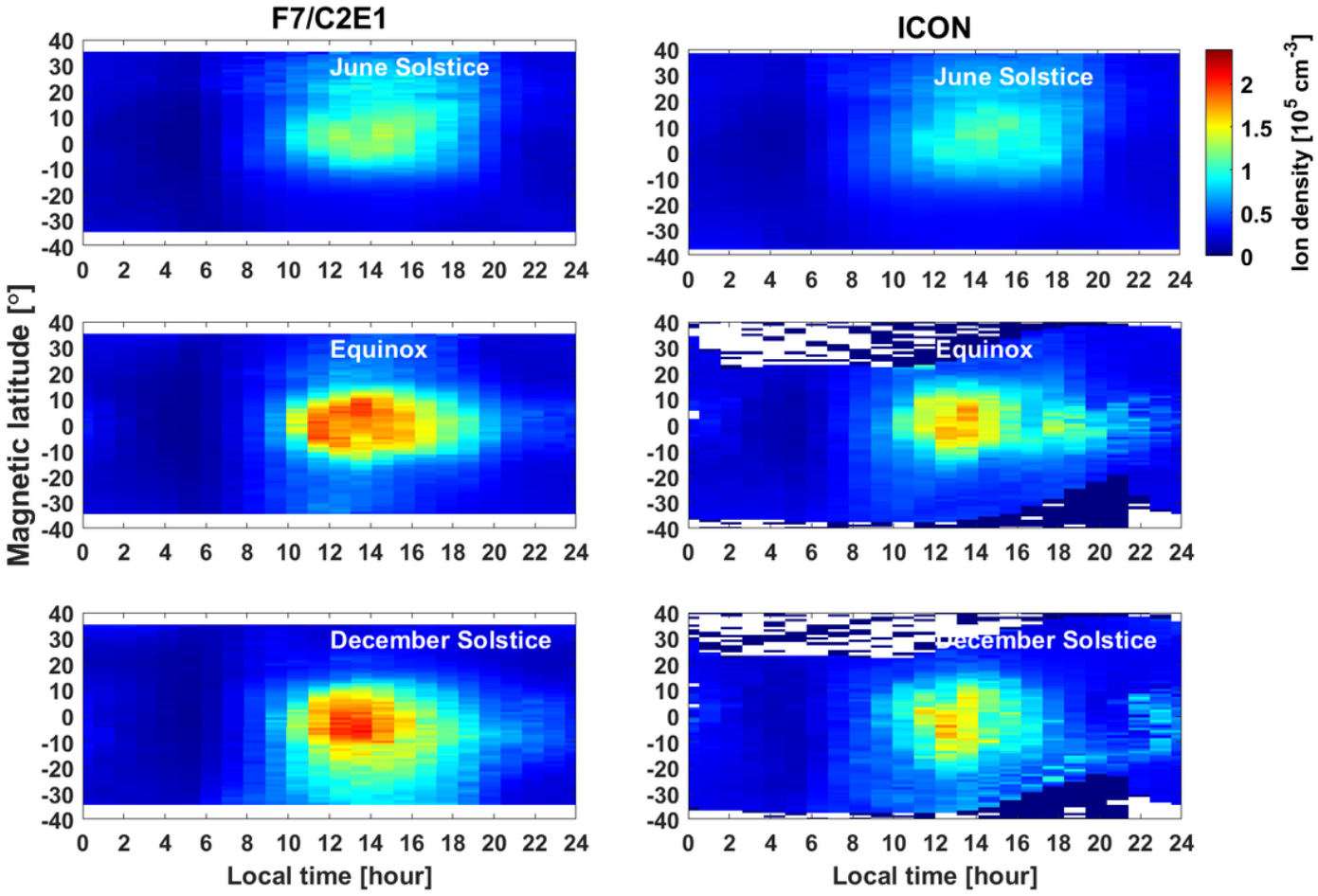

Figure 5

The magnetic latitude and local time distributions of the topside average ion densities observed by F7/C2E1 and ICON.

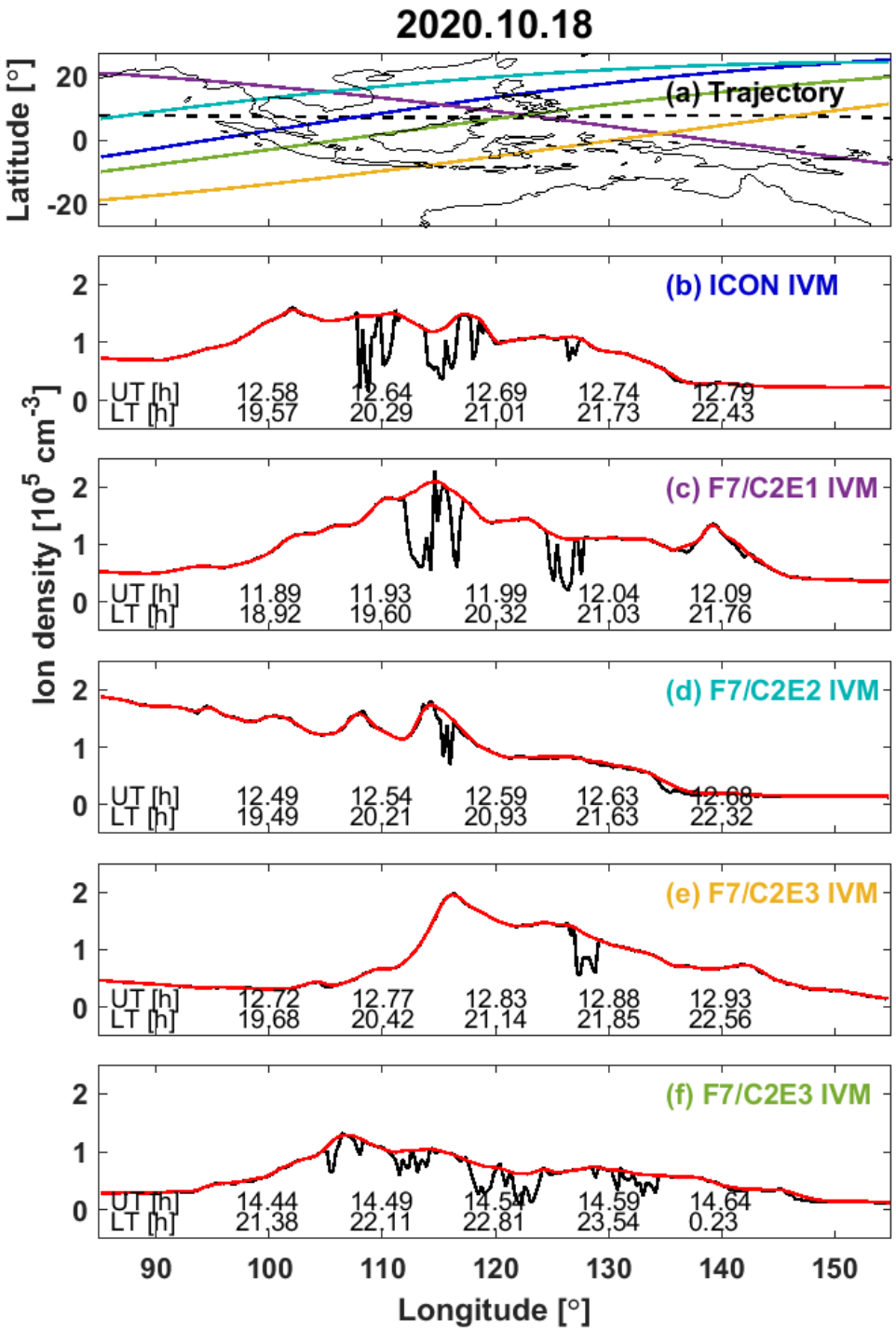

Figure 6

The evolution of equatorial plasma bubbles measured by ICON and F7/C2 IVM around Taiwan on 18 October 2020. Panel (a) shows the ICON and F7/C2 orbits while the magnetic equator is shown with by black dashed line. The black and red curves indicate the measured ion density and calculated background density from (b) ICON IVM, (c) F7/C2E1 IVM, (d) F7/C2E2 IVM (e) F7/C2E3 IVM (~2100 LT), and (f) F7/C2E3 (~2200 LT), respectively.

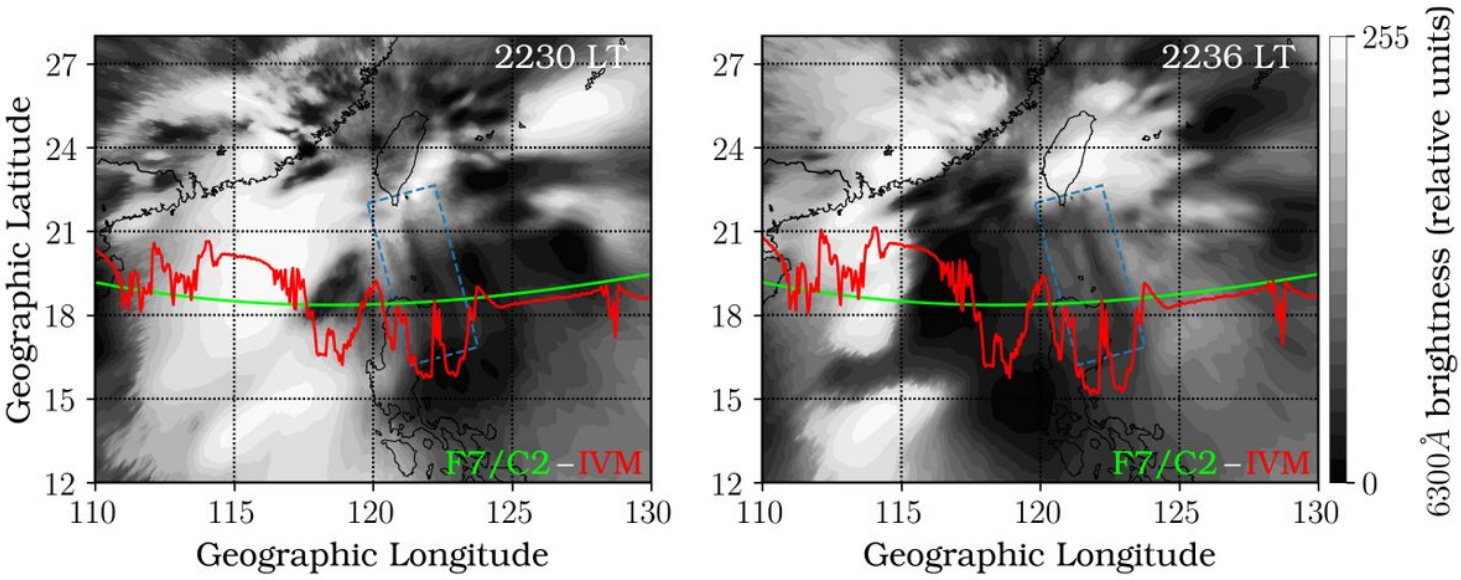

Figure 7

Simultaneous observations of unwarped OI 630.0 nm airglow images with the ion density of (left) F7/C2E2 at 2230 LT and (right) F7/C2E3 at 2236 LT on 18 October 2020.

Supplementary Files

This is a list of supplementary files associated with this preprint. Click to download.

- GraphicalAbstract.png